ISTITUTO NAZIONALE DI FISICA NUCLEARE

Laboratori Nazionali di Frascati

INFN-22-05-LNF
14-11-2022

High electric field induced damage using a pulsed THz source: a new technique to test metallic surfaces

S. Macis[1,2], A. D' Elia[2,3], A. Irizawa[4,*], M.Carillo[5,6], B. Spataro[2], Z. Ebrahimpour[2], L. Mosesso[1], J.S. Rezvani[7], S. Lupi[1,2] and A. Marcelli[2,3]

[1]Department of Physics, Università Sapienza, P.le Aldo Moro 5, 00185 Rome, Italy
[2]INFN, Laboratori Nazionali di Frascati, Via Enrico Fermi 54, 00044, Frascati (Rome), Italy
[3]Rome International Centre for Materials Science Superstripes, Via dei Sabelli 119A, 00185 Rome, Italy
[4]The Institute of Scientific and Industrial Research (ISIR), Osaka University, 8-1 Mihogaooka, Ibaraki, Osaka 5670047, Japan
[5]Department of Basic and Applied Sciences for Engineering, Sapienza University, via A. Scarpa 14, 00161 Roma, Italy
[6]INFN–Sezione di Roma, P.le Aldo Moro 2, Roma 00185, Italy
[7]Sezione Fisica, Scuola di Scienze e Tecnologie, Università di Camerino, via Madonna delle Carceri, Camerino (MC) 62032, Italy.

Abstract

We used the ISIR Free Electron Laser (FEL) of the Osaka university to irradiate with THz pulses the surface of a Cu thick sample and MoO_3 films with different thicknesses deposited on Cu. The linearly polarized, intense and coherent THz radiation pulses induced extensive and visible damages as a function of the irradiation angle. This approach allowed to define a protocol of irradiation in order to study the damage as a function of the beam intensity, the number of shots, the angle of incidence and the polarization of the radiation. This irradiation procedure applies to the sample surface under study an electric field gradient that may reach values as high as few GV/m. This original approach makes possible to test in a reproducible way films or the surface of a bulk material to a high electric field gradient on a well-defined region of the surface.

**now at SR Center, Research Organization of Science and Technology, Ritsumeikan University, 1-1-1 Nojihigashi, Kusatsu 525-8577, Shiga, Japan*

1. Introduction

One of the most stimulating R&D of the accelerating technology is the developing of improved RF cavities. This R&D is mainly triggered by the demand to run accelerators with higher accelerating gradients [1]. RF devices working at gradients greater than 100 MV/m or higher could be successfully used for the next generation of linear accelerators planned for research applications, but much more to design smaller and less expensive industrial equipment, e.g., to be used in biomedical and food industries.
To improve established RF technologies based on copper devices, we oriented our research to improve the properties of OFHC copper coated with harder and conductive coatings. DEMETRA, NUCLEAAR and IMPACT INFN projects, funded by 5th national scientific committee (CSN5), have been dedicated to the growth and characterization of thin films of Transition Metal Oxides (TMOs) deposited on copper to improve the surface properties of accelerating cavities [2]. These coatings may allow to optimize the properties of accelerating RF devices reducing field emission, breakdown rate, and thermal damage in the presence of high electric fields [3].
In order to test the damage induced by a high electric field on RF devices with coated surfaces, instead of assembling a real cavity and starting the long processes of cleaning, baking, conditioning and applying a high power to measure the effective operational performances, we developed a reliable measurements protocol based on the irradiation of a high intensity coherent THz radiation beam. We used the ISIR Free Electron Laser (FEL) in Osaka as the THz radiation source. In this way the beam it is intense, highly polarized and coherent [3,4].
The testing protocol consisted in the reproducible irradiation of the sample surface by several THz pulses with different intensity and time structure. This approach makes possible to generate and measure the surface damage on a well-defined sample region and, in addition, allows to measure and compare copper with different coated surfaces in a reproducible way.
We calculated that with the ISIR figures, the electric field on the sample surface may reach values as high as 5 GV/m, i.e., allowing to compare the aftermath of the exposure to electric fields gradients higher than the target electric fields required by the most demanding RF devices.
In this contribution we present results of irradiations performed on different samples: a Cu substrate and different MoO_3 films deposed on copper. We observed and characterized the damage as a function of beam intensity, number of shots, angle of incidence, and polarization of the radiation.

2. Experimental Layout

THz radiation was generated by the ISIR Free Electron Laser, a coherent source where a LINAC accelerates an electron beam up to 15 MeV [4]. The pulsed electron beam travels inside an undulator that emits radiation in the THz range. A series of optics extract the highly coherent beam outside the accelerator hutch, focusing it on the sample position for different kinds of experiments.

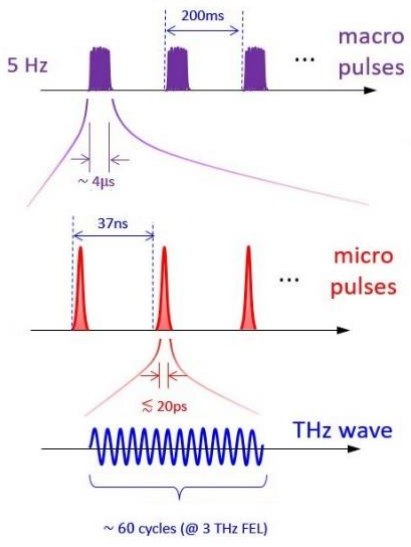

Figure 1. The electron beam structure of the ISIR FEL. In the top panel is showed the macro pulse structure, in the center the micro pulse (20 ps long) and in the bottom the oscillating wave at 3 THz inside the micro pulse.

As showed in Fig. 1, the time-structure of the emitted radiation is characterized by "macro" and "micro" pulses. The macro pulse is 4 μs long and has a repetition rate of 5 Hz. Each macro pulse contains 108 micro pulses (repetition rate of 27 MHz) each one 20 ps long. For these irradiation experiments we measured with the calibrated Coherent® energy meter the energy of a single macro pulse (12 mJ). The focal spot of this THz beam after the undulator and the optical system has a Gaussian distribution with a $\sigma \approx 75$ μm and we estimated that 95.5% of the beam intensity lies in a circular spot with a diameter of ~260 μm. The electric field generated at the centre of the spot was estimated to be ~5 GV/m [3,4].

3. Irradiation experiments

Different tests were performed on different samples to clarify if the observed damage

- changes with the incidence angle;
- varies with the beam intensity, i.e., with the macro-pulse energy;
- depends by the number of shots, i.e., with the number of macro-pulses;
- is affected by irradiation with s or p polarization.

All tests were performed using p-polarization as depicted in Figure2, except where specified otherwise. In this configuration the electric field has the component perpendicular to the sample's surface. In our experimental layout, the sample may rotate along the axis forming an angle α with the surface plane. At variance, in the s-wave configuration the electric field lies on the surface and is not affected by any rotation of the sample along the same axis.

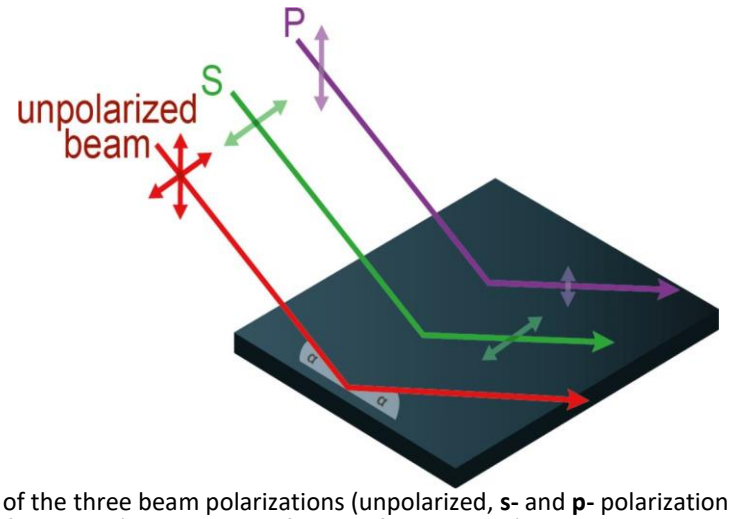

Figure 2. Representation of the three beam polarizations (unpolarized, **s-** and **p-** polarization) respect to the irradiated surface. The **p-wave** configuration (used in most of the performed tests) has the beam polarization perpendicular to the sample surface. When $0° < \alpha < 90$, the electric field has a component perpendicular to the surface, which is higher at lower angles. Using the **s-wave** configuration the polarization is lying in the surface plane and for any α value, the electric field remains parallel to the surface.

4. Raman characterization

After experiments samples were sent back to Italy where visible images of the irradiated areas were collected. The damaged areas have been analyzed *ex-situ* at the Laboratori Nazionali di Frascati using Raman Spectroscopy. With its high spatial resolution this is a suitable technique to characterize the observed copper damage, identifying the chemical composition of the surface point by point and/or mapping the damaged areas. Measures were performed with a green laser (532 nm) with a 20X magnification objective and a 5 μm diameter spot.

The full damaged area of any sample was visualized with Raman maps. This technique consists in defining a grid whose entries are different positions on the sample's surface. For each position (i.e., points of the grid) a Raman spectrum is acquired. By selecting a characteristic feature of the Raman spectrum, e.g., the peak that corresponds to CuO or Cu_2O. etc., it is possible to visualize the intensity distribution of any selected feature on the investigated sample surface. This approach makes

possible to map the different chemical species distributed on the sample surface, adding spatial information to intensity and chemical information provided by the technique.
To evaluate the copper damage, we looked at the oxides generated by the irradiation. Two type of copper oxides are mainly observed after the irradiation process: copper (II) oxide (CuO) and copper (I) oxide (Cu_2O) [5]. Due to heating inhomogeneities in the irradiated area, the two oxides appear in different regions where damage occurs. In the left panel in Figure 3 we compare the two spectra of the copper oxides observed in two locations within the same damaged area (that showed in Figure 7). The intensity of the peak at 230 cm^{-1} (black arrow) was used to study the Cu_2O spatial distribution, while for CuO oxide we used the intensity of the peak at 300 cm^{-1} (red arrow) [5]. In the right panel in Figure 3 is reported the Raman spectra of a disordered phase of MoO_3 deposited on Cu. We used the wide Raman peak at about 800 cm^{-1} to build the intensity maps of MoO_3 in the coated samples.

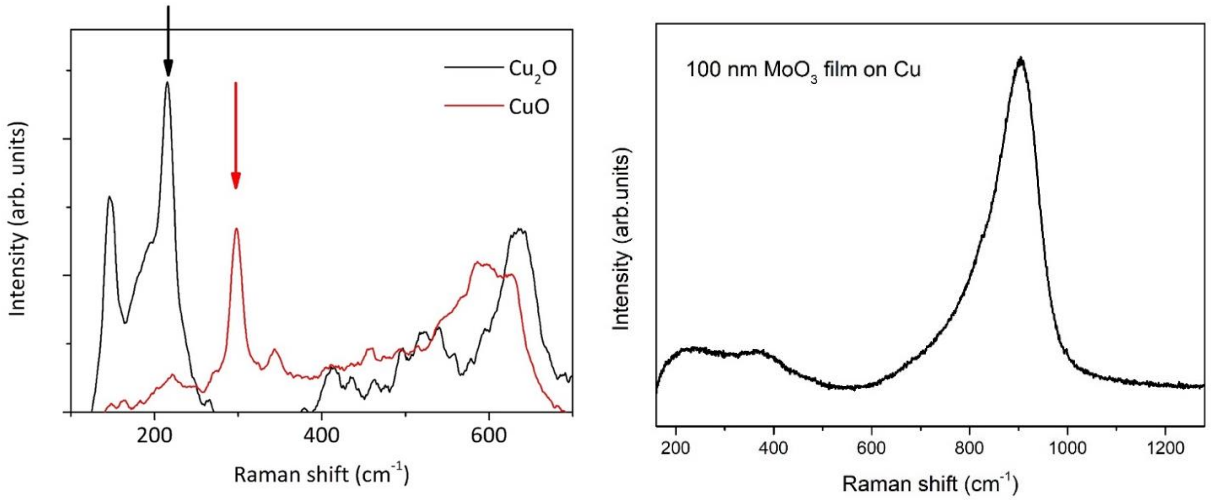

Figure 3. Left: comparison of the Raman spectra of the two copper oxides observed in the irradiated regions. Cu_2O is mainly formed in the external corona surrounding the focal spot, while CuO oxide is detected in the central region. The red and black arrows point features used to map CuO and Cu_2O distributions. Right: The Raman spectrum of a MoO_3 film (100 nm) deposed on Cu.

5. Measurements as a function of the incidence angle

In this section are showed tests performed on copper and copper coated by molybdenum oxides as a function of the incidence angle (respect to the surface normal). All irradiations showed in this section have been performed at the maximum power of the ISIR FEL, i.e., with the macro pulse of 12 mJ in the **p**-polarization. The total number of macro pulses illuminating the sample for each test i.e., the total number of shots, is set constant to 5000. In the table below are listed all tests performed vs. the incidence angle.

Table 1: Irradiations performed as a function of the incident angle and number of shots. Highlighted in green tests performed on Cu while the others refer to MoO_3 films on copper.

Sample	*Incidence angle [°]*	*Damage*	*Number of shots*
Cu substrate	0	Not observable	5000
	20	yes	5000
	40	yes	5000
	60	yes	5000
MoO_3 85nm	0	Not observable	5000
	20	Not observable	5000
	40	yes	5000
	60	yes	5000
MoO_3 100nm	40	yes	5000
	60	yes	5000

We report that for the Cu substrate and the 85 nm thick film of MoO_3 for angles of incidence 0° and 20°, no radiation damage is observed. This means that in the area we illuminated no visible damage has been detected. The results suggests that if damage occurs it is absent or negligible. Since the

lack of damage is associated with small angles of incidence respect to the surface normal, the polarization component perpendicular to the surface is very small and the component of the electric field oriented perpendicular to the surface of the sample plays an important role when damage occurs.

5.1 Irradiation of a Cu thick substrate

The first characterizations refer to copper substrates about 10 mm thick. For all samples the first figure shows the photograph of the exposed area, while the second figure show an image of the central region of the damaged area combined with two Raman maps of the copper oxides detected in this region: the Cu_2O distribution whose intensity is given by the integral of the Raman peak in the range 135 and 160 cm^{-1}, and the CuO distribution whose intensity is associated to the integral of the Raman peak between 280 and 318 cm^{-1}. All maps generated by this procedure, show the intensity as a color scale.

5.1.1 Irradiation at the incidence angle of 20°

Figure 4: Large view optical image of the damaged area (the image is ~1x1.5 mm).

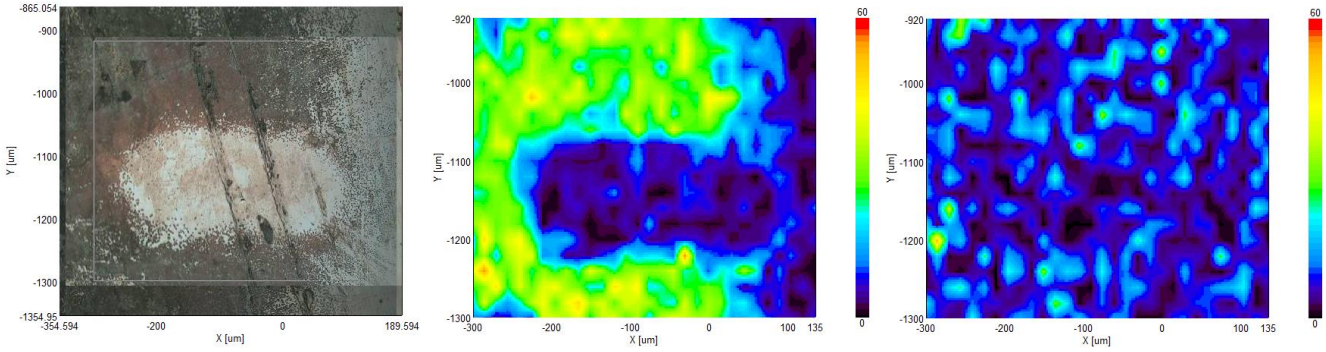

Figure 5: (left) Microscope image of the central region of the damaged area showed in Fig. 4, obtained with irradiation at 20° of incidence angle, 100% of FEL power and 5000 shots. On the central- and right-panel the two Raman maps of the copper oxides: the Cu_2O and the CuO, respectively.

5.1.2 Irradiation at the incidence angle of 40°

Figure 6: Large view optical image of the damaged area (the image is ~1x1.5 mm).

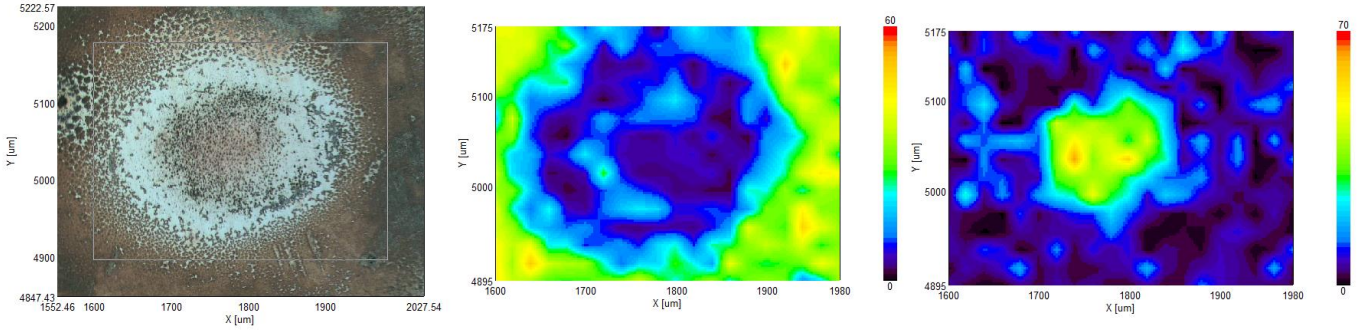

Figure 7: (left) Microscope image of the central region of the damaged area showed in Fig. 6, obtained with irradiation at 40° of incidence angle, 100% of FEL power and 5000 shots. On the central- and right-panel the two Raman maps of the copper oxides: the Cu_2O and the CuO, respectively.

5.1.3 Irradiation at the incidence angle of 60°

Figure 8: Large view optical image of the damaged area (the image is ~1x1.5 mm).

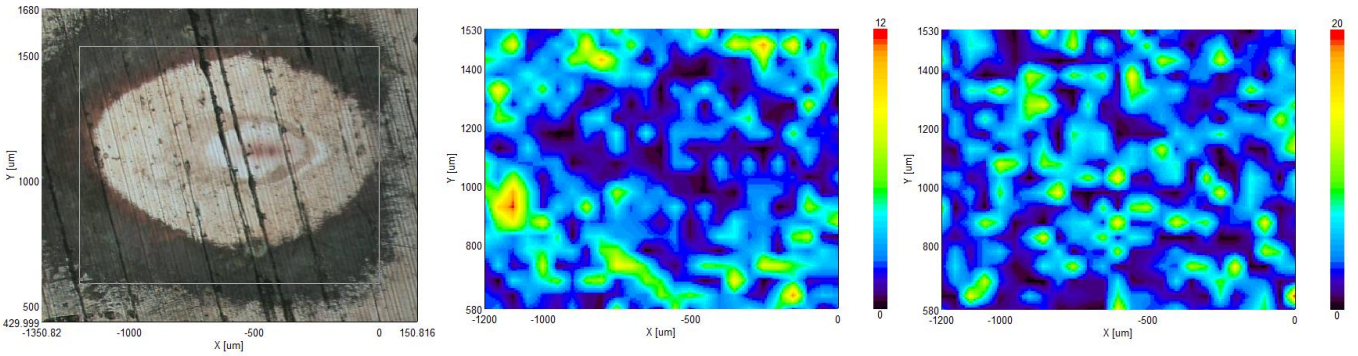

Figure 9: (left) Microscope image of the central region of the damaged area showed in Fig. 8, obtained with irradiation at 60° of incidence angle, 100% of FEL power and 5000 shots. On the central- and right-panel the two Raman maps of the copper oxides: the Cu_2O and the CuO, respectively.

5.2 MoO_3 film 85 nm thick on Cu

After the copper substrate we characterized molybdenum oxide films. In this section, and in the following for these films, the first figure shows the photograph of the exposed area, while the second figure show an image of the central region of the damaged area combined with Raman maps of CuO using the intensity of the peak at 300 cm^{-1} and MoO_3 using the wide Raman peak at about 800 cm^{-1} detected in the coated samples.

5.2.1 Irradiation at the incidence angle of 40°

Figure 10: Large view optical image of the damaged area (the image is ~1x1.5 mm).

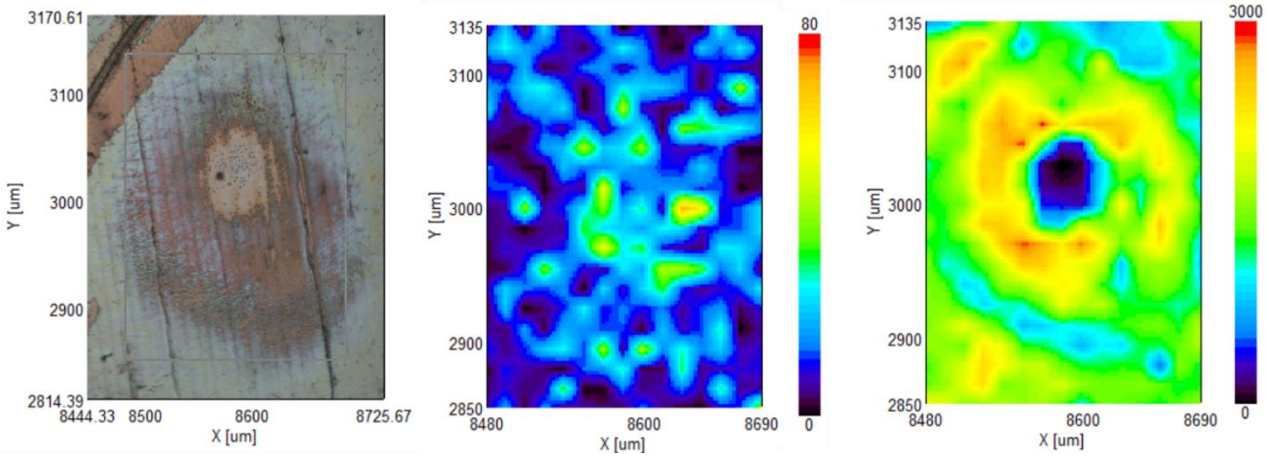

Figure 11: (left) Microscope image of the central region of the damaged area showed in Fig. 10, obtained with irradiation at 40° of incidence angle, 100% of FEL power and 5000 shots. On the central- and right-panel the two Raman maps of the CuO and the amorphous MoO_3, respectively.

5.2.2 Irradiation at the incidence angle of 60°

Figure 12 MoO_3: Large view optical image of the damage (the image is ~ 1x1.5 mm).

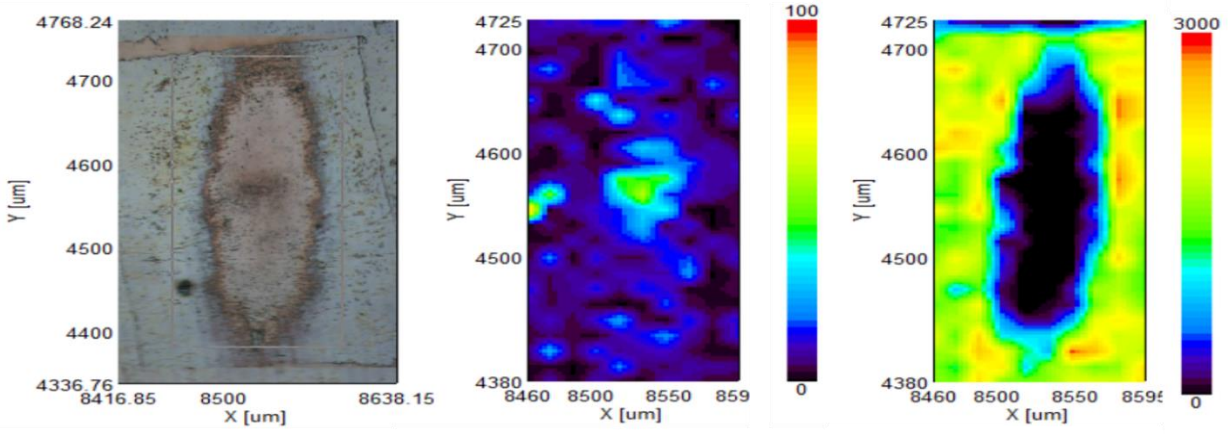

Figure 13: (left) Microscope image of the central region of the damaged area showed in Fig. 12, obtained with irradiation at 60° of incidence angle, 100% of FEL power and 5000 shots. On the central- and right-panel the two Raman maps of the CuO and the amorphous MoO_3, respectively.

5.3 MoO_3 film 100 nm thick on Cu

5.3.1 Irradiation at the incidence angle of 40°

Figure 14: Large view optical image of the damage (the image is ~ 1 x1.5 mm).

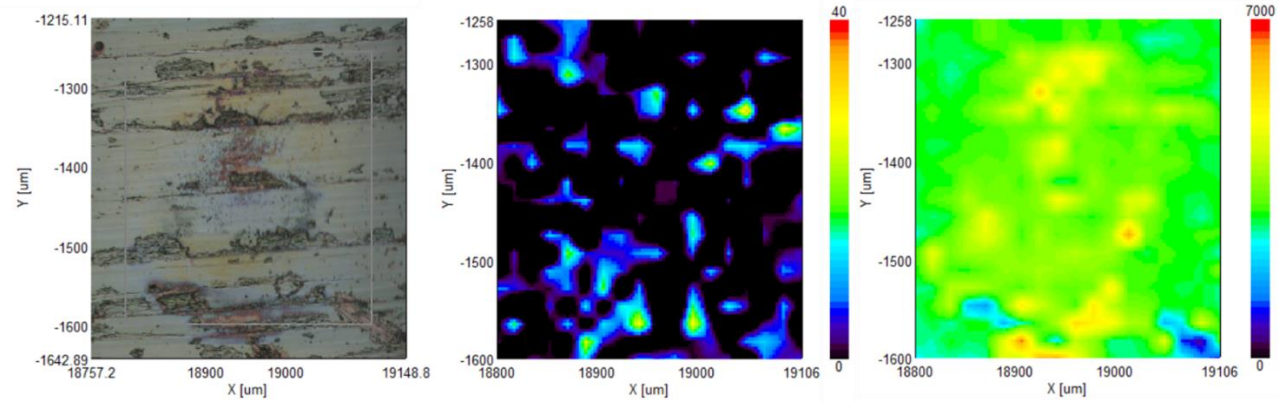

Figure 15: (left) Microscope image of the central region of the damaged area showed in Fig. 14, obtained with irradiation at 40° of incidence angle, 100% of FEL power and 5000 shots. On the central- and right-panel the two Raman maps of the CuO and the amorphous MoO_3, respectively.

5.3.2 Incidence angle 60°

Figure 16: Large view optical image of the damage (the image is ~1x1.5 µm).

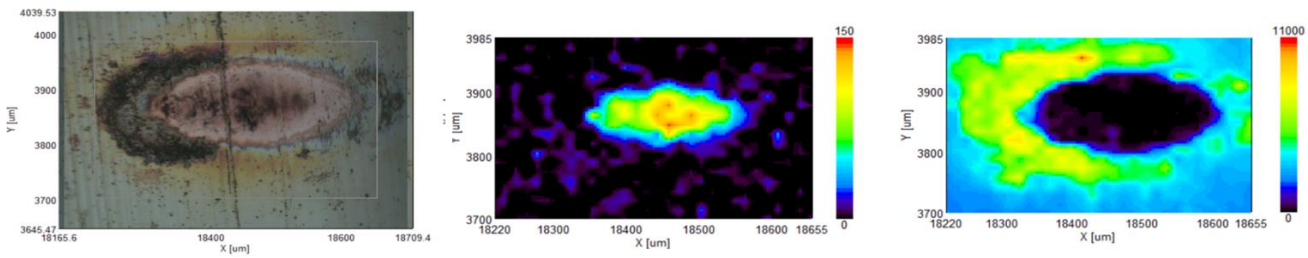

Figure 17: (left) Microscope image of the central region of the damaged area showed in Fig. 16, obtained with irradiation at 60° of incidence angle, 100% of FEL power and 5000 shots. On the central- and right-panel the two Raman maps of the CuO and the amorphous MoO_3, respectively.

5.4 Induced damage as a function of the incident energy

In this section we show results of irradiations performed as a function of the incident energy in the **p**-polarization to investigate the dependence of the surface damage from the incident energy. To this purpose we tuned the energy of the macro pulse using filters that reduced the total incident energy by 50% and 90%.

Table 2: Irradiations performed as a function of the incident energy. Highlighted in green tests performed on Cu while the others refer to MoO_3 films on copper.

Sample thickness [nm]	Energy of macro pulse [mJ]	Incidence angle [°]	Damage	Number of shots
Cu substrate	12	40	yes	5000
	6	40	yes	5000
	1.2	40	Not observable	5000
	12	60	yes	5000
	6	60	yes	5000
	1.2	60	Not observable	5000
MoO_3 100 nm	12	40	yes	5000
	6	40	yes	5000
	1.2	40	Not observable	5000
	12	60	yes	5000
	6	60	yes	5000
	1.2	60	Not observable	5000

No damage has been detected on both Cu and MoO_3 film for the incident energy of 1.2 mJ, at any angle of incidence, a value probably too small to induce any damage.

5.5 Irradiation of a Cu substrate about 10 mm thick

5.5.1 Incidence energy = 12 mJ; incidence angle 40°

Figure 18: Large view optical image of the damage (the image is ~1x1.5 µm).

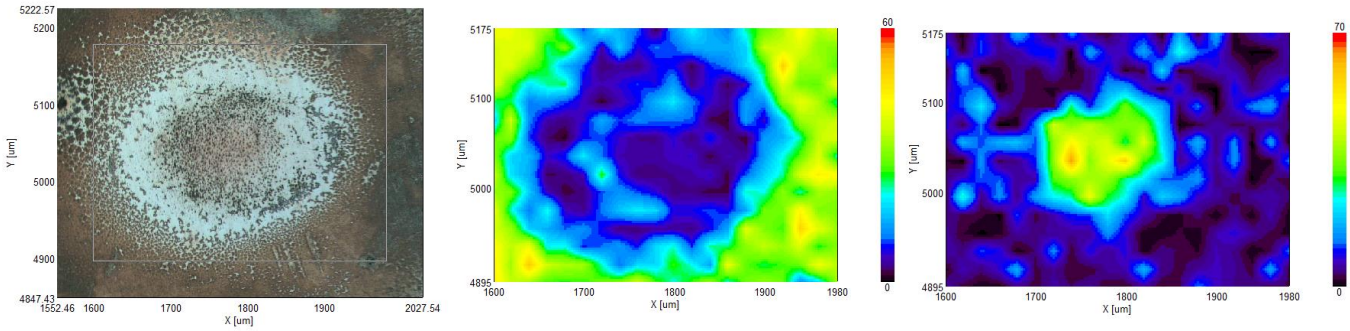

Figure 19: (left) Microscope image of the central region of the damaged area showed in Fig. 18, obtained with irradiation at 40° of incidence angle, incidence energy 12 mJ and 5000 shots. On the central- and right-panel the two Raman maps of the copper oxides: the Cu_2O and the CuO, respectively.

5.5.2 Incidence energy = 6 mJ; incidence angle 40°

Figure 20: Large view optical image of the damage (the image is ~1x1.5 mm).

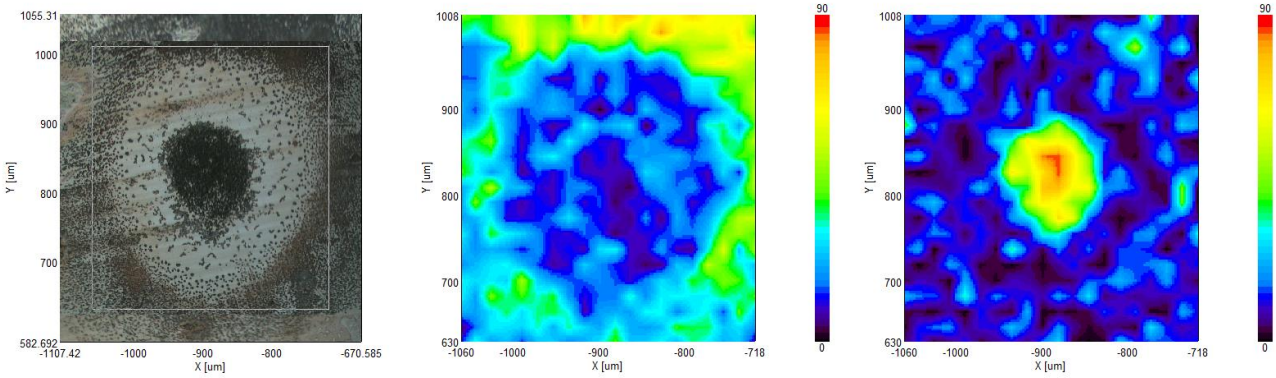

Figure 21: (left) Microscope image of the central region of the damaged area showed in Fig. 20, obtained with irradiation at 40° of incidence angle, incidence energy 6 mJ and 5000 shots. On the central- and right-panel the two Raman maps of the copper oxides: the Cu_2O and the CuO, respectively.

5.5.3 Incidence energy = 12 mJ; incidence angle 60°

Figure 22: Large view optical image of the damage (the image is ~1x1.5 mm).

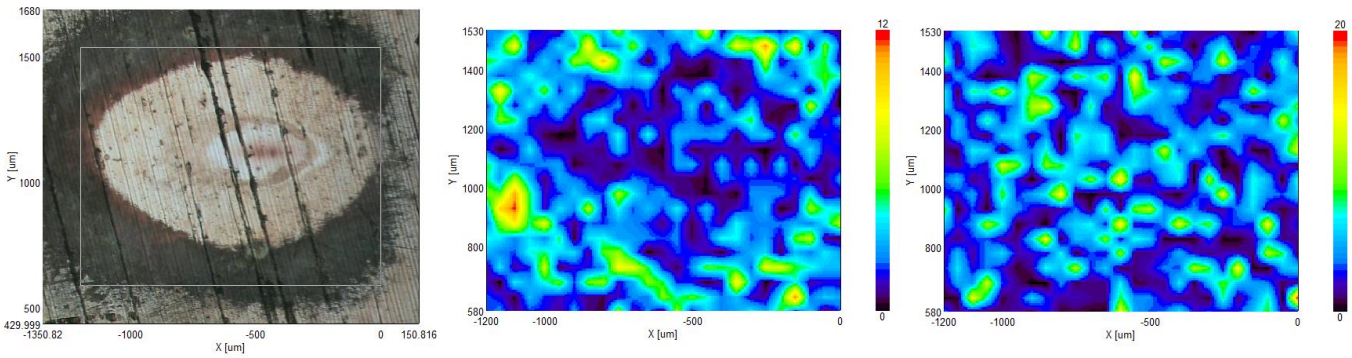

Figure 23: (left) Microscope image of the central region of the damaged area showed in Fig. 22, obtained with irradiation at 60° of incidence angle, incidence energy 12 mJ and 5000 shots. On the central- and right-panel the two Raman maps of the copper oxides: the Cu_2O and the CuO, respectively.

5.5.4 Incidence energy = 6 mJ; incidence angle 60°

Figure 24: Large view optical image of the damage (the image is ~1x1.5 mm).

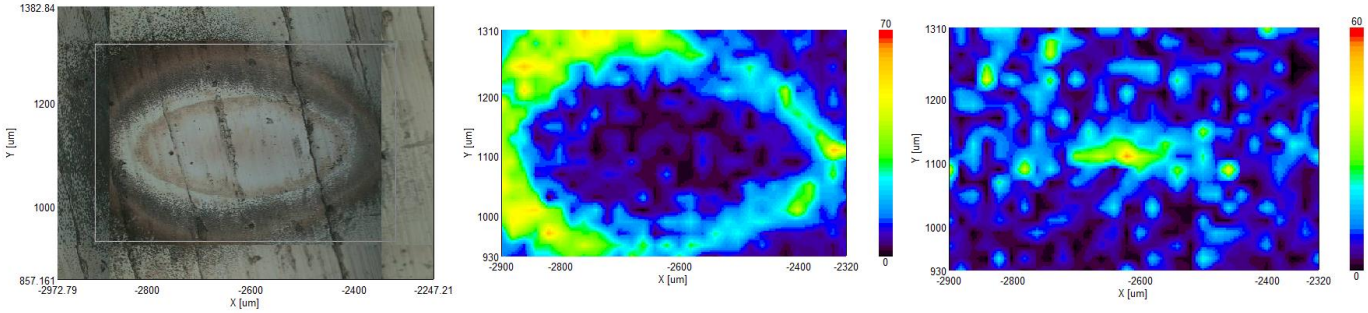

Figure 25: (left) Microscope image of the central region of the damaged area showed in Fig. 24, obtained with irradiation at 60° of incidence angle, incidence energy 6 mJ and 5000 shots. On the central- and right-panel the two Raman maps of the copper oxides: the Cu_2O and the CuO, respectively.

5.6 MoO_3 film 100 nm thick on Cu

5.6.1 Incidence energy = 12 mJ; incidence angle 40°

Figure 26: Large view optical image of the damage (the image is ~1x1.5 mm).

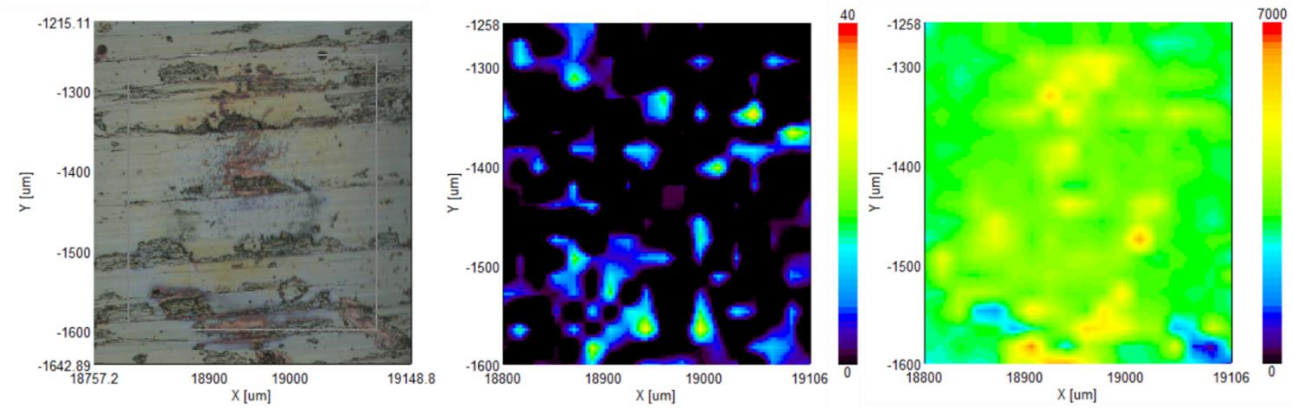

Figure 27: (left) Microscope image of the central region of the damaged area showed in Fig. 26, obtained with irradiation at 40° of incidence angle, incidence energy 12 mJ and 5000 shots. On the central- and right-panel the two Raman maps of the CuO and the amorphous MoO_3, respectively.

5.6.2 Incidence energy = 6 mJ; incidence angle 40°

Figure 28: Large view optical image of the damage (the image is ~1x1.5 mm).

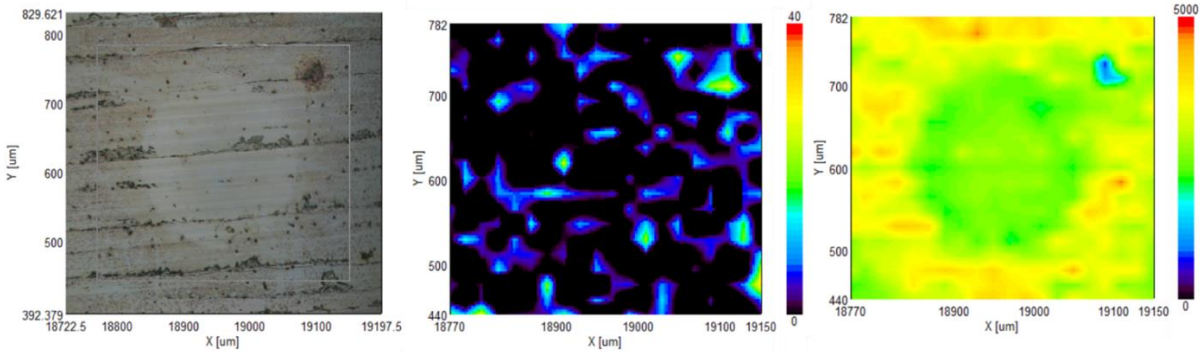

Figure 29: (left) Microscope image of the central region of the damaged area showed in Fig. 28, obtained with irradiation at 40° of incidence angle, incidence energy 6 mJ and 5000 shots. On the central- and right-panel the two Raman maps of the CuO and the amorphous MoO_3, respectively.

5.6.3 Incidence energy = 12 mJ; incidence angle 60°

Figure 30: Large view optical image of the damage (the image is ~1x1.5 mm).

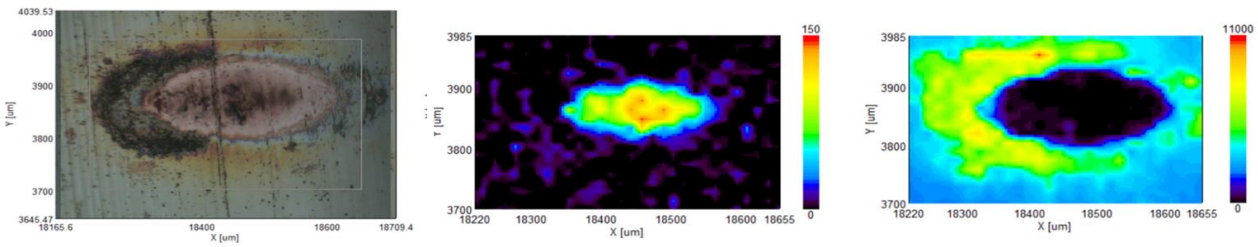

Figure 31: (left) Microscope image of the central region of the damaged area showed in Fig. 30, obtained with irradiation at 60° of incidence angle, incidence energy 12 mJ and 5000 shots. On the central- and right-panel the two Raman maps of the CuO and the amorphous MoO_3, respectively.

5.6.4 Incidence energy = 6 mJ; incidence angle 60°

Figure 32: Large view optical image of the damage (the image is ~ 1x1.5 mm).

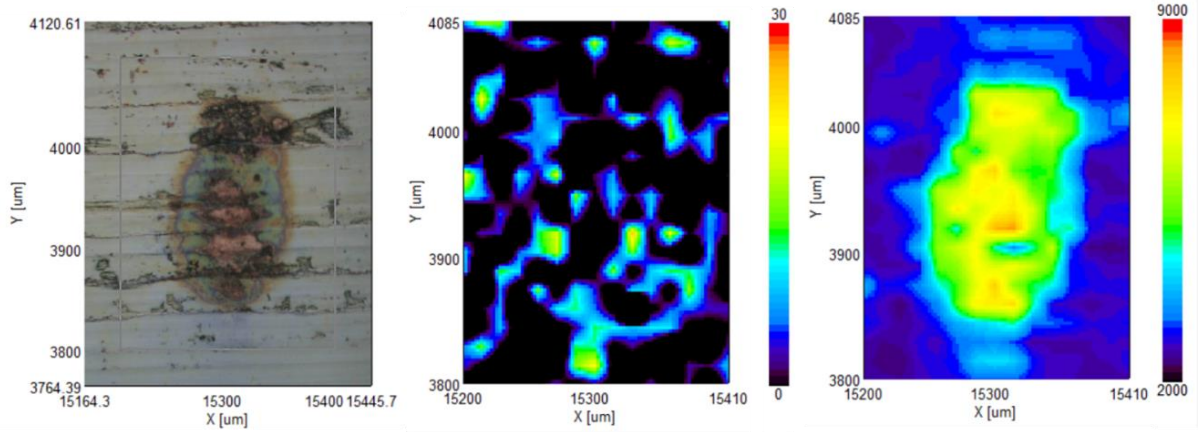

Figure 33: (left) Microscope image of the central region of the damaged area showed in Fig. 32, obtained with irradiation at 60° of incidence angle, incidence energy 6 mJ and 5000 shots. On the central- and right-panel the two Raman maps of the CuO and the amorphous MoO_3, respectively.

5.7 Tests performed changing the shots number

In this section we reported the results of the tests performed as a function of the shots number. We observed and characterized the damage as a function of the number of shots maintaining constant the angle of incidence, the polarization of the radiation (*p*-polarization) and the incident energy. The latter was fixed to the maximum value available by the ISIR FEL, i.e., 12 mJ.

Table 3: List of the test performed as a function of the shots number. Highlighted in green tests performed on Cu while the others refer to MoO_3 films on copper.

Sample thickness [nm]	Number of shots	Incidence angle [°]	Energy of macro pulse [mJ]	Damage
Cu substrate	10000	40	12	yes
	5000	\\	\\	yes
	2000	\\	\\	yes
	1000	\\	\\	yes
	500	\\	\\	Not observable
	200	\\	\\	Not observable
	100	\\		Not observable
MoO_3 100 nm	10000	40	12	Not observable
	5000	\\	\\	yes
	2000	\\	\\	Not observable
	1000	\\	\\	Not observable
	500	\\	\\	Not observable
	200	\\	\\	Not observable
	100	\\	\\	Not observable

For the Cu sample, surface damages are not observable for shots number < 1000. The result suggests a threshold behaviour, but further analysis have to be performed to confirm this behaviour. In the case of MoO_3 film, a visible damage appears only for 5000 shots confirming that these oxides coatings are more resistant to irradiation respect to bare copper. However, also at 10000 shots damage was not detected. Additional tests are planned to clarify this result.

5.8. Irradiation of a Cu substrate about 10 mm about 10 mm

5.8.1 Irradiation with 10000 shots

Figure 34: Large view optical image of the damage (the image is ~1x1.5 mm).

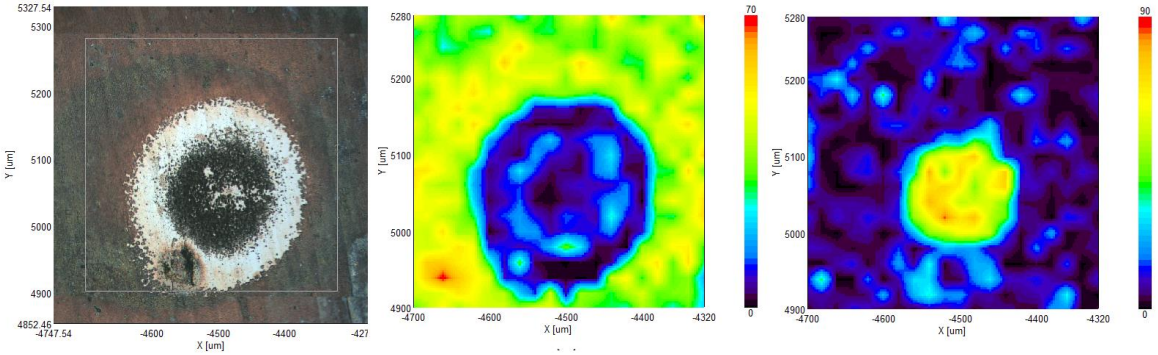

Figure 35: (left) Microscope image of the central region of the damaged area showed in Fig. 34, obtained with irradiation at 40° of incidence angle, 100% of FEL power and 10000 shots. On the central- and right-panel the two Raman maps of the copper oxides: the Cu_2O and the CuO, respectively.

5.8.2 Irradiation with 5000 shots

Figure 36: Large view optical image of the damage (the image is ~1x1.5 mm).

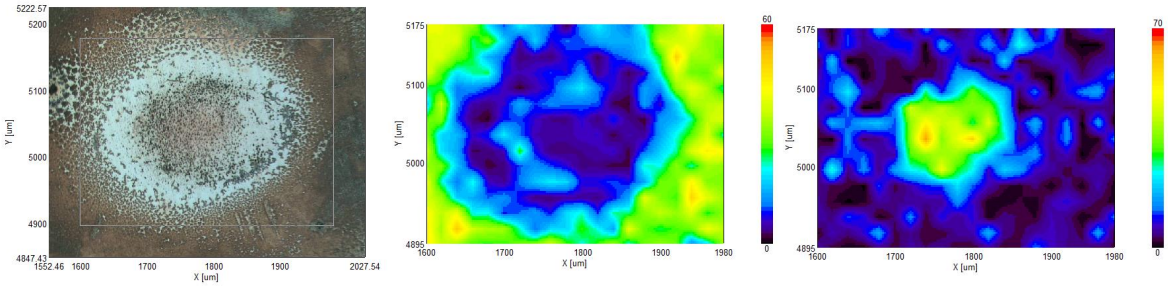

Figure 37: (left) Microscope image of the central region of the damaged area showed in Fig. 36, obtained with irradiation at 40° of incidence angle, 100% of FEL power and 5000 shots. On the central- and right-panel the two Raman maps of the copper oxides: the Cu_2O and the CuO, respectively.

5.8.3 Irradiation with 2000 shots

Figure 38: Large view optical image of the damage (the image is ~1x1.5 mm).

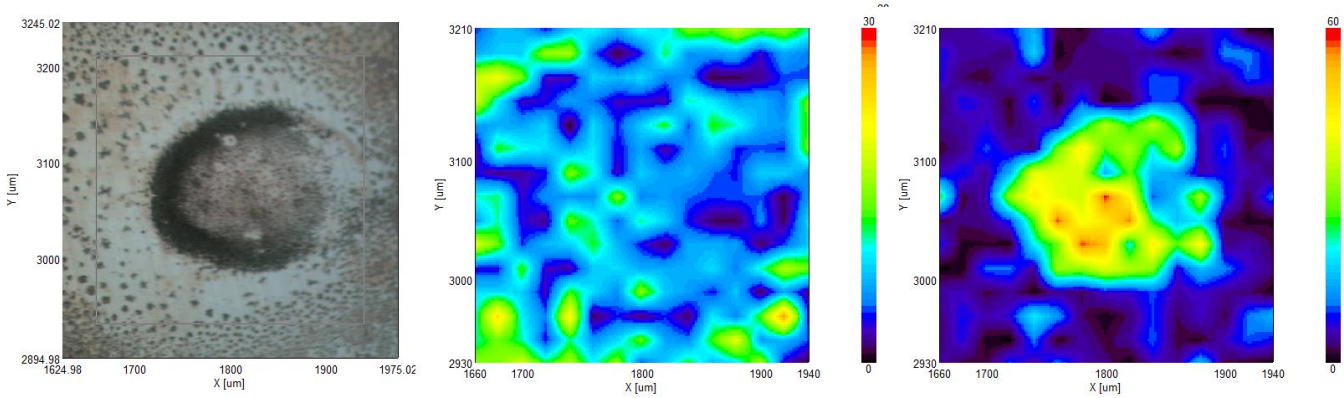

Figure 39: (left) Microscope image of the central region of the damaged area showed in Fig. 38, obtained with irradiation at 40° of incidence angle, 100% of FEL power and 2000 shots. On the central- and right-panel the two Raman maps of the copper oxides: the Cu_2O and the CuO, respectively.

5.8.4 Irradiation with 1000 shots

Figure 40: Large view optical image of the damage (the image is ~1x1.5 mm).

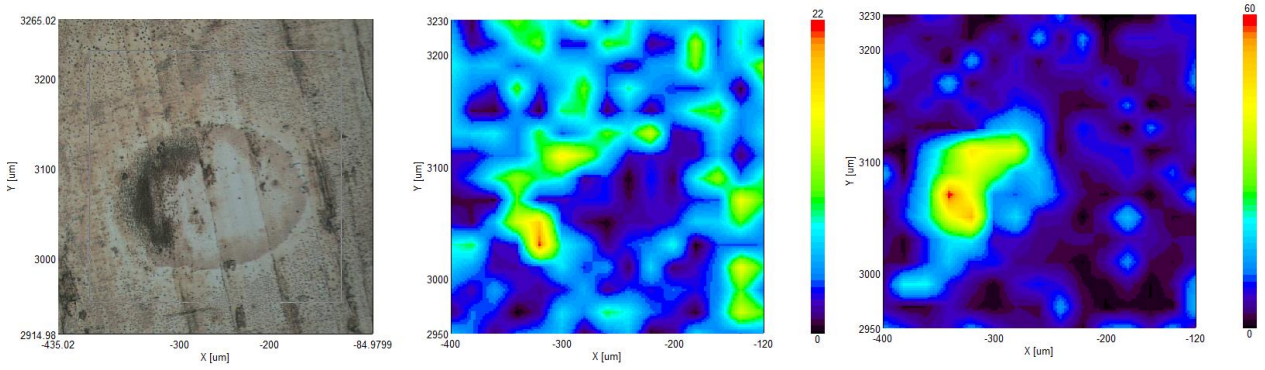

Figure 41: (left) Microscope image of the central region of the damaged area showed in Fig. 40, obtained with irradiation at 40° of incidence angle, 100% of FEL power and 1000 shots. On the central- and right-panel the two Raman maps of the copper oxides: the Cu_2O and the CuO, respectively.

5.9 Irradiation of a MoO_3 film 100 nm thick on Cu

5.9.1 Irradiation with 5000 shots

Figure 42: Large view optical image of the damage (the image is ~1x1.5 mm).

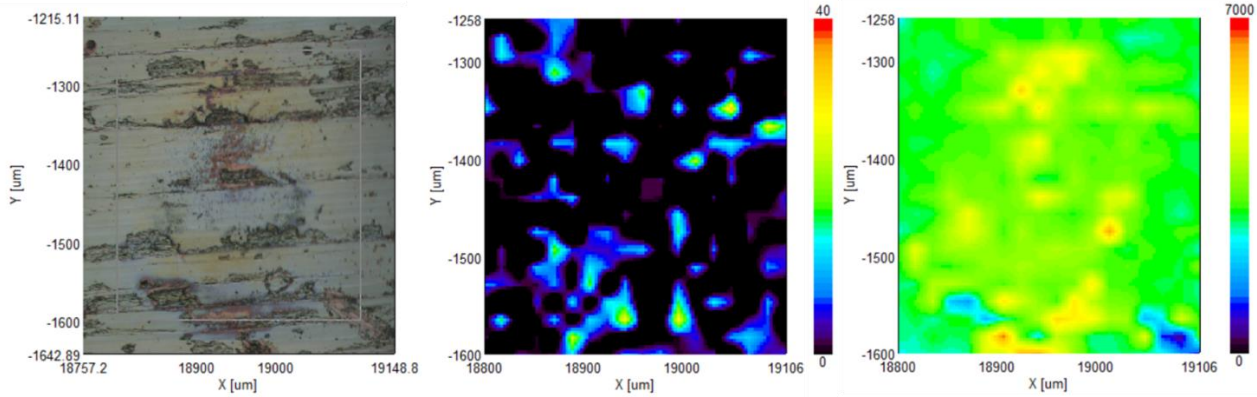

Figure 43: (left) Microscope image of the central region of the damaged area showed in Fig. 42, obtained with irradiation at 40° of incidence angle, incidence energy 12 mJ and 5000 shots. On the central- and right-panel the two Raman maps of the CuO and the amorphous MoO_3, respectively.

5.10 Tests with s-polarization

We performed also tests irradiating the samples with a THz beam at the incidence angle of 40°, at the pulse energy of 12 mJ, 5000 shots in the **s-**polarization layout. In this optical configuration no damage has been detected on both Cu and films of MoO_3 (100 nm thick) deposed on copper. We hope that this behaviour is due to the orientation of the electric field respect to the sample surface. In the case of irradiation using the *s*-polarization the electric field always lays in the sample's surface plane. This result and the observation of a trend for the damage irradiation with the *p*-polarization point out that the electric filed component directed perpendicular to the sample surface is associated to the observed damage vs. energy and vs. angle.

Discussion

The results of the irradiation performed using coherent THz radiation showed in this report point out important phenomena occurring both on copper surfaces and films of molybdenum oxides deposed on a copper substrate.
Looking at the damaged areas observed on the copper substrate, Raman maps of copper oxides clearly show how CuO and Cu_2O occurs in different regions of the exposed region. CuO is mainly present in the central spot where higher temperatures are reached by the metal, while Cu_2O is mainly detected in the external corona of the spot.
Tests as a function of the incidence angle on the Cu substrate return damages compatible with previous tests always performed at ISIR. Increasing the incidence angle, the damaged area increases, and the irradiated spot broadens. The maximum damage (associated to the largest damaged area) occurs between 40° and 60°. At normal incidence no damage is detectable because almost all radiation is reflected by metallic surfaces.
Different results are obtained irradiating coated surfaces. Both 85 nm and 100 nm thick MoO_3 films show damaged regions (see visible photographs and Raman maps) and the partial removal of the

film occurs in the central region of the spot. The removal of the film was not observed in previous irradiation tests. The different behavior could be due to the ~20% increase of the energy of the THz beam in the irradiation presented in this report.
Irradiation tests as a function of the incident energy were performed for the first time. Data regarding the Cu substrate point out a reduction of the size of the damaged area with the reduction of the incident energy. Tests performed at 100% and 50% intensity show a clear oxidation of copper with both CuO and CO_2. On the other hand, using only 10% of the beam intensity no oxidation or damage is detectable. An intensity threshold for the copper surface damage may exist, suggesting a non-linear behavior that has to be confirmed by additional tests.
The irradiations were performed at the incidence angle of 40° and 60°. Among these two angles a significant difference between damaged areas occurs. As an example, at 60° using 6 mJ of incident energy the external corona is smaller and closer to the center of the spot compared to the damage observed at the incidence angle of 40°.
We also studied the damage as a function of the shots number, i.e., the number of the incident macro pulses. On Cu the damage showed a monotonic trend as a function of the number of shots, suggesting that the effect is cumulative. Below 1000 shots no damage was detected on the surface. For the 100 nm MoO_3 film a visible damage is observed only with 5000 shots. Due to the increased damage resistance films of MoO_3 deposed Cu exhibit a higher damage threshold. The damage at 1000 shots is not detectable, but additional tests need to be carried out.
We performed for the first-time tests using the **s-**wave polarization at the incidence angle of 40° at the maximum power for both copper and MoO_3 100 nm thick films. No damage was detected for both samples. The results confirm that the electric field component perpendicular to the surface plays a fundamental role to induce a surface damage using highly coherent THz radiation.
Damage induced by a strong EM field on metallic surfaces has been already observed [6-8] and reflection and absorption processes of a high-intensity optical laser pulse by an extremely smooth metal surface have been studied [9-12].
Laser-induced damaged morphologies and their cumulative effects induced by single pulses have been discussed by Agranat *et al.* [13]. The damage mechanism induced by a single THz pulse was attributed to the thermal expansion of the thin Al film causing its debonding from the substrate, cracking, and ablation [13]. However, the damage pattern induced by multiple terahertz pulses at fluences below the damage threshold is quite different from that observed in single-pulse experiments. Moreover, it has been recently pointed out the occurrence of an angular dependent reproducible damage induced by multiple high-intensity THz pulses on metallic copper surfaces. [3] In this contribution authors showed that increasing the incidence angles and with multiple shots ($>10^3$) and a fluence of 12,7 J/cm^2 per pulse the damage increases. The evaluated temperature reached at the metallic surface matches the experimental results and points out that the increase in absorption at high incidence angles is the responsible of the damage and, also of the copper oxidation. Actually, images of the damaged surfaces show that for incidence angles > 20°, the temperature reached can be higher than the melting temperature of copper. These effects are in agreement with previous reports in the optical frequency range, described in terms of higher absorbance, increased angle of incidence [14] and multiple shots irradiation [15].
Other studies modelled the damage using the mechanism of ultrafast laser ablation of solids and the underlying processes on a broad range of timescales from femtosecond to nanosecond, i.e., from the initial energy absorption to the final material removal. [16]
The interaction of pulses of THz radiation has been also explained using the universal polariton model [17]. This model of laser-induced breakdown deals with the self-organization mechanism inducing a grating on the surface by the interference of the incident wave with the surface polaritons excited by that wave. However, all the above treatments do not consider electric-related effects, e.g., discharges and/or breakdowns occurring in air due to light pulses, and also do not explain the angular dependence, the differences observed using light with different polarizations and the negligible or no damages on samples coated by thin Mo oxides films.

Acknowledgments

We acknowledge the Ministero degli affari esteri e della cooperazione internazionale for support, within the framework of the Italian-Chinese collaborative research in 3D graphene and Italian-Japanese bilateral project "*Spettroscopia THz lineare, non lineare e risolta in tempo con sorgenti di radiazione di ultima generazione*".

We acknowledge Ivan Davoli of Tor Vergata University for the evaporation setup. We also acknowledge the Osaka University for providing beamtime at the ISIR facility.

References

[1] R.B. Palmer, Acceleration theorems, AIP Conference Proceedings 335, 90–100 (2008) https://doi.org/10.1063/1.48253.

[2] S. Macis, C. Aramo, C. Bonavolontà, G. Cibin, A. D'Elia, I. Davoli, M. De Lucia, M. Lucci, S. Lupi, M. Miliucci, A. Notargiacomo, C. Ottaviani, C. Quaresima, M. Scarselli, J. Scifo, M. Valentino, P. De Padova, and A. Marcelli, MoO_3 films grown on polycrystalline Cu: Morphological, structural, and electronic properties, J. Vacuum Science & Technology A 37(2), 021513 (2019)

[3] S. Macis, L. Tomarchio, S. Tofani, S.J. Rezvani, L. Faillace, S. Lupi, A. Irizawa, A. Marcelli, Angular Dependence of Copper Surface Damage Induced by an Intense Coherent THz Radiation Beam. Condens. Matter 5, 16 (2020)

[4] A. Irizawa, S. Suga, T. Nagashima, A. Higashiya, M. Hashida and, S. Sakabe, Laser-induced fine structures on silicon exposed to THz-FEL. Applied Physics Letters, 111, 251602 (2017)

[5] L. George, A. Gupta, P.R. Shaina, N. Das Gupta, M. Jaiswal, Mechanical tearing of graphene on an oxidizing metal surface, Nanotechnology. 26 (2015) https://doi.org/10.1088/0957-4484/26/49/495701.

[6] Y. Jee, M.F. Becker, R.M. Walser, Laser-induced damage on single-crystal metal surfaces. J. Opt. Soc. Am. B 5, 648 (1988)

[7] M.D. Forno, V. Dolgashev, G. Bowden, C. Clarke, M. Hogan, D. McCormick, A. Novokhatski, B. O'Shea, B. Spataro, S. Weathersby, et al. High gradient tests of metallic mm-wave accelerating structures. Nucl. Instrum. Methods Phys. Res. Sect. A Accel. Spectrometers Detect. Assoc. Equip. 864, 12–28 (2017)

[8] M.D. Forno, V. Dolgashev, G. Bowden, C. Clarke, M. Hogan, D. McCormick, A. Novokhatski, B. O'Shea, B. Spataro, S. Weathersby, et al. Measurements of electron beam deflection and RF breakdown rate from a surface wave guided in metallic mm-wave accelerating structures. Phys. Rev. Accel. Beams 21, 091301 (2018)

[9] R. Fedosejevs, R. Ottmann, R. Sigel, G. Kühnle, S. Szatmári, F.P. Schäfer, Absorption of subpicosecond ultraviolet laser pulses in high-density plasma. Appl. Phys. B 50, 79–99 (1990)

[10] M.B. Agranat, N.E. Andreev, S.I. Ashitkov, M.E. Veisman, P.R. Levashov, A.V. Ovchinnikov, D.S. Sitnikov, V.E. Fortov, K.V. Khishchenko, Determination of the transport and optical properties of a nonideal solid-density plasma produced by femtosecond laser pulses. JETP Lett. 85, 271–276 (2007)

[11] A. Ng, P. Celliers, A. Forsman, R.M. More, Y.T. Lee, F. Perrot, M.W.C. Dharma-Wardana, G.A. Rinker, Reflectivity of intense femtosecond laser pulses from a simple metal. Phys. Rev. Lett. 72, 3351 (1994)

[12] M. Cerchez, R. Jung, J. Osterholz, T. Toncian, O. Willi, P. Mulser, H. Ruhl, Absorption of ultrashort laser pulses in strongly overdense targets. Phys. Rev. Lett. 100, 245001 (2008)

[13] M.B. Agranat, O.V. Chefonov, A.V. Ovchinnikov, S.I. Ashitkov, V.E. Fortov, Damage in a thin metal film by high-power terahertz radiation. Phys. Rev. Lett. 120, 085704 (2018)

[14] A.Y. Vorobyev, C. Guo, Reflection of femtosecond laser light in multipulse ablation of metals. J. Appl. Phys. 110, 043102 (2011)

[15] Y. Miyasaka, M. Hashida, T. Nishii, S. Inoue, S. Sakabe, Derivation of effective penetration depth of femtosecond laser pulses in metal from ablation rate dependence on laser fluence, incidence angle, and polarization. Appl. Phys. Lett. 106, 013101 (2015)

[16] B. Rethfeld, D.S. Ivanov, M.E. Garcia and S.I. Anisimov, Modelling ultrafast laser ablation, J. Phys. D: Appl. Phys. 50, 193001 (39pp) (2017)

[17] V.S. Makin and R.S. Makin, The universal character of the breakdown of condensed media by powerful terahertz radiation and the Abbe criterion, J. Optical Technology 87 (1) 2020